Achieving high-efficiency non-doped blue organic light-emitting diodes: charge-balance control of bipolar blue fluorescent materials with reduced hole-mobility†

Chih-Chin Chi,[a] Chih-Long Chiang,[ab] Shun-Wei Liu,[ac] Han Yueh,[d] Chin-Ti Chen*[ab] and Chao-Tsen Chen*[d]

Received 11th February 2009, Accepted 11th May 2009
First published as an Advance Article on the web 19th June 2009
DOI: 10.1039/b902910a

We found an unusual way in improving electroluminescence efficiency of blue organic light-emitting diodes (OLEDs). Two electron deficient 4,5-diazafluorene- or di(2,2′-pyridyl)-containing blue fluorophores, **PhSP$_{N2}$DPV** (4,5-diaza-2′-diphenylamino-7′-(2,2″-diphenylvinyl)-9,9′-spirobifluorene) and **PhF$_{py2}$DPV** (N-[7-(2,2-diphenylvinyl)-9,9′-di(2,2″-pyridyl)-2-fluorenyl]-N,N-diphenylamine), were synthesized and characterized for non-doped blue OLEDs. Whereas **PhF$_{py2}$DPV** OLED performs ordinarily, **PhSP$_{N2}$DPV** OLED outperforms previously known **PhSPDPV** (2-diphenylamino-7-diphenylvinyl-9,9′-spirobifluorene) OLED significantly: maximum external quantum efficiency of ~5% (4.6% at 20 mA cm^{-2}) and the peak electroluminance of 60510 cd m^{-2} (1810 cd m^{-2} at 20 mA cm^{-2}) *versus* 3.4% (2.9% at 20 mA cm^{-2}) and 33020 cd m^{-2} (910 cd m^{-2} at 20 mA cm^{-2}) of **PhSPDPV** OLED. We attribute the superior performance of **PhSP$_{N2}$DPV** OLED to the good charge balancing, which is in turn due to the very low hole mobility of **PhSP$_{N2}$DPV**. The experimental results reveal that the electron-deficient moiety, 4,5-diazafluorene or di(2,2′-dipyridyl), increases electron affinity but reduces the hole mobility. Electron mobility, determined by time-of-flight (TOF) method, is 5×10^{-5} and 5×10^{-4} cm^2 V^{-1} s^{-1} (at an electric field of 4.9×10^5 V cm^{-1}) for **PhSP$_{N2}$DPV** and **PhF$_{py2}$DPV**, respectively. Surprisingly, they are not higher than 8×10^{-4} cm^2 V^{-1} s^{-1} of nonpolar **PhSPDPV**. On the other hand, hole mobility is 2×10^{-6} and 2×10^{-4} cm^2 V^{-1} s^{-1} for **PhSP$_{N2}$DPV** and **PhF$_{py2}$DPV**, respectively, and they are both significantly lower than 6×10^{-3} cm^2 V^{-1} s^{-1} of **PhSPDPV**. For **PhSP$_{N2}$DPV** and **PhF$_{py2}$DPV** bipolar blue fluorophores, we have demonstrated that electron-transporting and light-emitting functions involve different molecular halves. The design of such molecular halves greatly facilitates the optical and electronic optimizations of fluorophores for high-performance OLEDs.

Introduction

Having a three times higher limit of theoretical electroluminescence (EL) efficiency, electrophosphorescence-based organic light-emitting diodes (OLEDs) are usually more favorable than electrofluorescence-based OLEDs.[1] However, blue electrofluorescence materials have revived and become highly demanded by the energy-saving solid-state lighting (SSL) of white OLEDs, which have been prevailed with troublesome electrophosphorescence materials recently.[2] In addition to the common problem of short operational lifetimes[2a,3] and the high material cost, electrophosphorescence-based OLEDs with acceptable blue color purity (a Commission Internationnale de l'Éclairage, CIE$_{x,y}$, coordinate of y <0.25) are relatively rare when compared with large numbers of green or red electrophosphorescence-based OLEDs.[4] Electrophosphorescence-based OLEDs showing true blue (CIE, coordinate of y <0.20) remain challenging and they always have not so high external quantum efficiency (η_{EXT}) of 5.8–8.5%.[5] More critically, blue electrophosphorescence-based OLEDs very often exhibit serious efficiency roll-off at elevated driving current density,[5] due to the T_1-T_1 annihilation nature of electrophosphorescence material. For practical SSL application, white OLEDs require electroluminance (L, or brightness) equal to or greater than 1000 cd m^{-2}, which is usually corresponding to a driving current density (J) over 20 mA cm^{-2} for electrophosphorescence-based OLEDs.[5] At such a current density, η_{EXT}s of blue electrophosphorescence-based OLEDs are usually low, often less than 5.5% of the conventional upper limit of the electrofluorescence efficiency of OLEDs.[6] Under such circumstances, electrophosphorescence-based blue OLEDs have very little advantage over electrofluorescence ones

In recent years, a growing number of literature examples can be found for blue or sky blue electrofluorescence-based OLEDs having a super high η_{EXT} of 5 ~ 8%.[7] These electrofluorescence-based OLEDs rival the best of true blue electrophosphorescence-based OLEDs. Except of bis(4-phenylquinoline)-based fluorophores,[7e] these super efficient fluorophores are either non-hetroatom-containing polycyclic aromatic hydrocarbons (PAHs) or arylamine-substituted PAHs, although insightful explanations of super high η_{EXT}'s are seldom reported.[7] Charge-transporting

[a]*Institute of Chemistry, Academia Sinica, Taipei, Taiwan, 11529, Republic of China. E-mail: cchen@chem.sinicaedu.tw; Fax: +886 2 27831237; Tel: +886 2 27898542*
[b]*Department of Applied Chemistry, National Chiao Tung University, Hsin-Chu, Taiwan, 30050, Republic of China*
[c]*Graduate Institute of Photonics and Optoelectronics and Department of Electrical Engineering, Taipei, Taiwan, 106, Republic of China*
[d]*Department of Chemistry, National Taiwan University, Taipei, Taiwan, 106, Republic of China. E-mail: chenct@ntu.edu.tw; Fax: +886 2 33664200*
† CCDC reference numbers 682902 and 682903. For crystallographic data in CIF or other electronic format see DOI: 10.1039/b902910a

and charge-balancing of OLEDs are two factors that seem to be crucial in high efficiency blue electrofluorescence-based OLEDs. Previous investigations have reported the injection of electrons or electron-transporting properties found for fluorene-based blue-emitting polymers and oligomers.[8] In addition, arylamine-substituted PAHs, such as 4,4′-bis[*N*-(1-naphthyl)-*N*-phenyl-amino]biphenyl (NPB), have been shown for similar hole- and electron-mobility.[9] However, the high energy gaps (>3 eV) essential for blue emission often result in low electron affinities (EAs < 2.5 eV) of these blue-light-emitting materials.[7e] This hampers charge injection, unbalances the charge carriers (hole and electron), and impairs the efficiency of blue OLEDs. Very often, elaboration of device fabrication (*i.e.*, doping process) and complication of device architecture (*i.e.*, multilayer device) are necessary to improve OLED performance.

In this paper, we report the synthesis, characterization, and EL property of a couple of novel blue fluorescent materials, 4,5-diaza-2′-diphenylamino-7′-(2,2″-diphenylvinyl)-9,9′-spirobi-fluorene (**PhSP$_{N2}$DPV**) and *N*-[7-(2,2″-diphenylvinyl)-9,9′-di(2,2″-pyridyl)-2-fluorenyl]-*N*,*N*-diphenylamine (**PhF$_{py2}$DPV**) (Scheme 1). Due to the electron-rich diphenylamine substituent and electron-deficient nitrogen-containing heterocyclic moieties, **PhSP$_{N2}$DPV** and **PhF$_{py2}$DPV** are bipolar in nature. They are the structurally modified version of virtually non-polar 2-diphenylamino-7-(2,2″-diphenylvinyl)-9,9′-spirobifluorene (**PhSPDPV**), an arylamine-substituted PAH previously known as the blue fluorophore for high efficiency non-dopant blue OLEDs.[10] Bipolar **PhSP$_{N2}$DPV** and **PhF$_{py2}$DPV** are special for two reasons. First, structural moieties associated with opposite polarity (electron-rich *vs.* electron-deficient) are separated from each other, *i.e.*, they are not connected to each other by π-conjugation. Second, as we demonstrate in this paper, decoupled molecular functions, light-emitting and electron-transporting, are realized in these bipolar blue emitters. For OLED application, we have found that **PhSP$_{N2}$DPV** is significantly more efficient than **PhSPDPV** for non-dopant blue OLEDs: maximum η_{EXT} is approaching 5.0% at about 100 cd m^{-2} (~1 mA cm^{-2}), 4.6% at 1000 cd m^{-2} (~19 mA cm^{-2}), and 4.2% at 3000 cd m^{-2} (~50 mA cm^{-2}). Furthermore, efficiency roll-off is much lighter than what is commonly seen in electrophosphorescence-based blue OLEDs. For fundamental significance, we have demonstrated that the charge balancing control of EL devices, namely the reduction of the hole mobility in matching the electron mobility, is effective in achieving high EL efficiency of the bipolar blue fluorophores.

Results and discussion

Synthesis and characterization

As shown in Scheme 2, the success to the preparation of **PhSP$_{N2}$DPV** and **PhF$_{py2}$DPV** hinges on the availability of

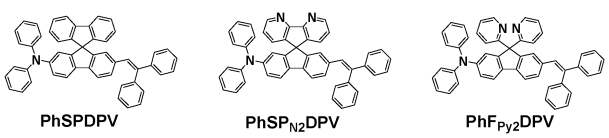

Scheme 1 Chemical Structures of **PhSPDPV**, **PhSP$_{N2}$DPV**, and **PhF$_{py2}$DPV**.

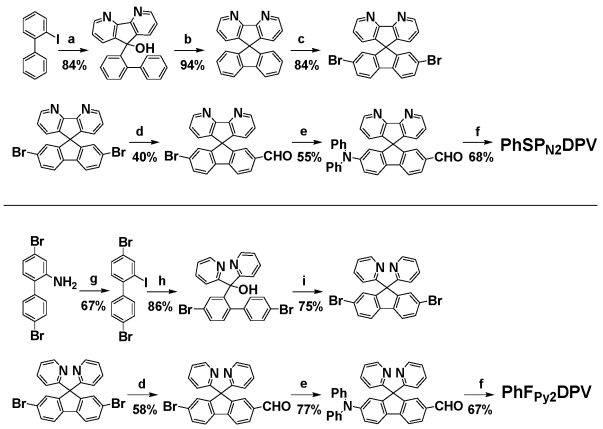

Scheme 2 Synthetic routes to **PhF$_{N2}$DPV** (top) and **PhF$_{py2}$DPV** (bottom). Reagents and conditions: (a) i. Mg, THF; ii. 4,5-diaza-9-fluorenone, THF, reflux; (b) H_2SO_4, HOAc, reflux; (c) Br_2, $FeCl_3$, CH_2Cl_2, rt.; (d) i. *n*-BuLi, THF, −78 °C; ii. DMF, rt.; (e) Ph_2NH, Cs_2CO_3, $Pd(OAc)_2$, P(*t*-Bu)$_3$, toluene, 120 °C; (f) NaH, $Ph_2CHPO(OEt)_2$, THF, reflux; (g) i. $NaNO_2$, 8 N HCl(aq), 0 °C; ii. KI, rt.; (h) i. *n*-BuLi, THF, −78 °C; ii. di-2-pyridyl ketone, THF, rt.; (i) i. NaH, THF, rt., then $SOCl_2$, 0 °C; ii. $AlCl_3$, CH_3NO_2, reflux. See the experimental section for full details.

dibromo-substituted species, 4,5-diaza-2′,7′-dibromo-9,9′-spirobifluorene and 2,7-dibromo-9,9′-di(2,2″-pyridyl) fluorene. Whereas 4,5-diaza-2′,7′-dibromo-9,9′-spirobifluorene was previously known,[11] 2,7-dibromo-9,9-di(2,2′-pyridyl)fluorene was synthesized through a four-step reaction. First, 2-iodo-4,4′-dibromobiphenyl was obtained by the iodination of 4,4′-dibromobiphenyl *via* Sandmeyer reaction of 2-amino-4,4′-dibromobiphenyl,[12] Second, 2-iodo-4,4′-dibromobiphenyl was mono-lithiated with a stoichiometric amount of *n*-butyllithium at −78 °C, followed by the reaction with di(2,2′-pyridyl)ketone to afford the key intermediate tertiary alcohol (carbinol). Unlike the one in the preparation of 4,5-diaza-9,9′-spirobifluorene, such carbinol failed to undergo ring-closure reaction with acids in the formation of 2,7-dibromo-9,9′-di(2,2″-pyridyl)fluorene due to the electron deficiency of di(2,2′-pyridyl) substituents. Such adverse situation was not found for the carbinol of 4,5-diaza-9,9′-spirobifluorene because of the non-resonanced *meta*-position of nitrogen atoms to the tertiary carbon of carbinol. The carbinol precursor of **PhF$_{py2}$DPV** was converted to tertiary halide by the treatment of thionyl chloride and then followed by the ring-closure *via* Friedel–Crafts alkylation in the presence of Lewis acid (aluminium trichloride in this case). In the synthesis of **PhSP$_{N2}$DPV** and **PhF$_{py2}$DPV**, the following three steps, mono-formylation, Pd-catalyzed aromatic amination, and Horner–Wadsworth–Emmons reaction (d, e, and f in Scheme 2), were very similar to those in the preparation of **PhSPDPV** and others.[10,13] Three blue emitters were fully characterized by ^{1}H and ^{13}C NMR, fast atom bombardment or electron impact-mass spectrometry (FAB-MS or EI-MS), and elemental analysis, and were consistent with proposed structures.

The ultimate structural evidence is from single crystal X-ray diffraction analysis.[14] A distinct structural difference of **PhSP$_{N2}$DPV** and **PhF$_{py2}$DPV** can be clearly seen in Fig. 1, namely the coplanar geometry of 4,5-diazafluorene moiety of the

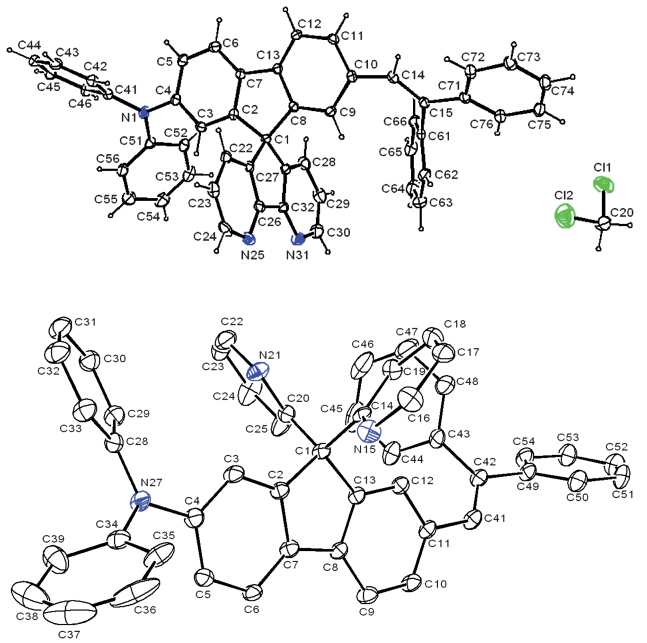

Fig. 1 The molecular structure of **PhSP$_{N2}$DPV** (top) and **PhF$_{py2}$DPV** (bottom) determined by X-ray diffraction analysis. Solvent molecule dichloromethane is included in the top figure and hydrogen atoms are removed for clarity in the bottom figure.

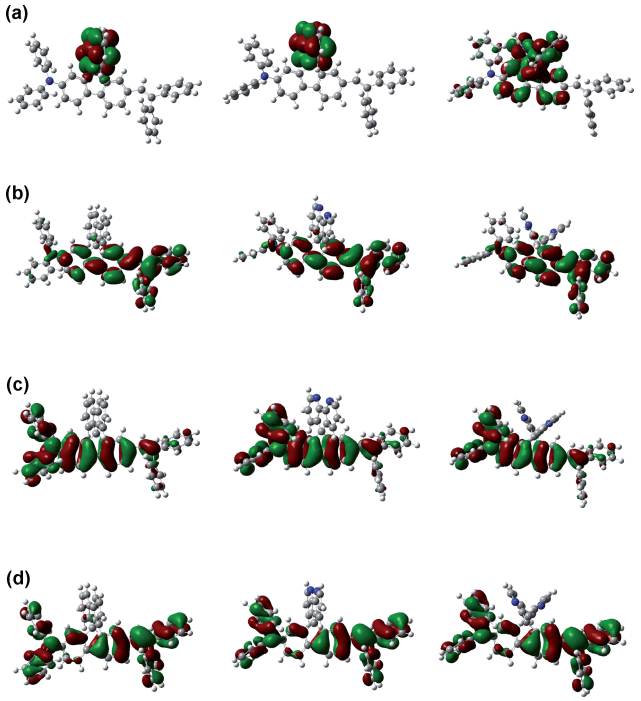

Fig. 2 Calculated frontier molecular orbital diagrams of **PhSPDPV**, **PhSP$_{N2}$DPV**, and **PhF$_{py2}$DPV** (from left to right) from DFT-B3LYP with 6–31G* basis set calculation: (a) LUMO +1; (b) LUMO; (c) HOMO; (d) HOMO −1.

former and the twisted non-planar conformation of di(2,2′-pyridyl) substituent of the latter. These structural features play an important role in affecting electron affinity, fluorescence quantum yield (Φ_f), charge carrier mobility, and eventually EL efficiency of OLEDs.

Theoretical estimation of molecular orbitals

The molecular structures of **PhSPDPV**, **PhSP$_{N2}$DPV**, and **PhF$_{py2}$DPV** were optimized by applying density functional theory (DFT) with the hybrid B3LYP functional and 6–31G* basis set, although single crystal X-ray structure of **PhSP$_{N2}$DPV** and **PhF$_{py2}$DPV** were the beginning structure in their structural optimization processes. With the optimized structure, calculations on the electronic ground states of **PhSPDPV**, **PhSP$_{N2}$DPV**, and **PhF$_{py2}$DPV** were processed using DFT with the hybrid B3LYP functional and 6–31G* basis set.[15] The singlet excited states of the three molecules were studied with time-dependent density functional theory (TDDFT) by using the hybrid B3LYP functional.[16] All calculations were preformed with a developmental version of Q-Chem.[17] We display a comparison of the corresponding HOMO −1, HOMO, LUMO, and LUMO +1 of the three blue emitters in S_0 state (Fig. 2). Because electronic excitation from the HOMO to the LUMO produces the first singlet excited state S_1 (a Frank–Condon excited state), the orbital features presented in Fig. 2 might provide important clues towards understanding the nature of optically accessible first excited state. The contour plots show that the HOMOs mainly consist of the π-orbitals of fluorene ring π-conjugated to the vinyl group, although a large extent of π-orbitals of the electronic donor, *N*,*N*-diphenylamino group, is involved as well. For the LUMOs, the orbitals mainly locate on diphenylvinylfluorene part of the molecule. π-Orbitals of *N*,*N*-diphenylamino electronic donor do not constitute LUMOs any more, although there remains certain π-orbital of the nitrogen atom of *N*,*N*-diphenylamino group. Such orbital involvement of HOMO and LUMO is nearly same in all three blue emitters. One can conclude that the photo-induced excitation (*i.e.*, absorption) or photo-induced relaxation (*i.e.*, emission) is most likely π–π* and moderate intramolecular charge-transfer (ICT) in nature. From our theoretical estimation, one should particularly note that the orbitals of the other molecular halve, *i.e.*, unsubstituted fluorenyl of **PhSPDPV**, 4,5-diazafluorenyl of **PhSP$_{N2}$DPV**, and di(2,2′-pyridyl) of **PhF$_{py2}$DPV**, little involve in the first singlet excited state (S_1) or Frank–Condon excited state, which is predominantly composed of LUMO in vacuum condition without the consideration of solvation effect.

Photophysical and electrochemical properties

The absorption and emission spectra of these blue emitters were studied in different organic solvents. As shown by data in Table 1, the absorption peak wavelength of three blue emitters exhibits insignificant solvent polarity dependence. Furthermore, as shown in Fig. 3, each of **PhSPDPV**, **PhSP$_{N2}$DPV** and **PhF$_{py2}$DPV** has very similar energy in Frank–Condon excitation when they are under the same solvent environment (polarity). The results can lead us to conclude a similar solvation effect between the ground and Frank–Condon excited states. In other words, the Frank–Condon excited state is subject to a rather small dipolar change with respect to the ground state. Such analysis is valid for all three blue emitters herein. This will not be

Table 1 Photophysical and electrochemical properties as well as energy levels of three blue emitters

	Solution			Solid state					
	λ_{max}^{ab} (nm)[a]	λ_{max}^{fl}, (nm)[a]	Φ_f (%)[b]	λ_{max}^{ab}, λ_{max}^{fl} (nm)	Φ_f (%)[b]	ΔE (eV)[c]	LUMO, HOMO (eV)[d]	$E_{1/2}^{red,1}$, $E_{1/2}^{oxd,1}$ (V)[e]	LUMO, HOMO (eV)[f]
PhSPDPV	383	458	60	383, 467	51	2.90	−2.58, −5.48	−2.72, 0.46	−2.08, −5.26
	386	468							
	378	491							
	385	454							
PhSP$_{N2}$DPV	388	466	66	390, 478	43	2.79	−2.70, −5.49	−2.63, 0.48	−2.17, −5.28
	379	501							
	383	462							
PhF$_{py2}$DPV	386	480	48	389, 480	42	2.78	−2.66, −5.44	−2.69, 0.43	−2.11, −5.23
	379	505							

[a] In toluene, chlorobenzene, and acetonitrile, respectively. [b] Φ_f's were determined by the integrating-sphere method and the solvent for solution Φ_f's was chlorobenzene. [c] ΔE is the band-gap energy estimated from the low energy edge of the absorption spectra of the thin film materials. [d] HOMO energy level was determined by low-energy photoelectron spectrometer (Riken-Keiki AC-2) and LUMO = HOMO + ΔE. [e] Electrochemical first reduction and first oxidation potentials with respect to the ferrocene/ferrocenium redox potential, which is 0.63 V *vs.* saturated Ag/$AgNO_3$, determined by differential pulsed voltammetry in a 0.1 M solution of $(Bu_4N)ClO_4$ in tetrahydrofuran. [f] LUMO = −4.8 eV − $E_{1/2}^{red,1}$ and HOMO = −4.8 eV − $E_{1/2}^{oxd,1}$, where 4.8 eV is the energy level of ferrocene/ferrocenium below the vacuum level.[18]

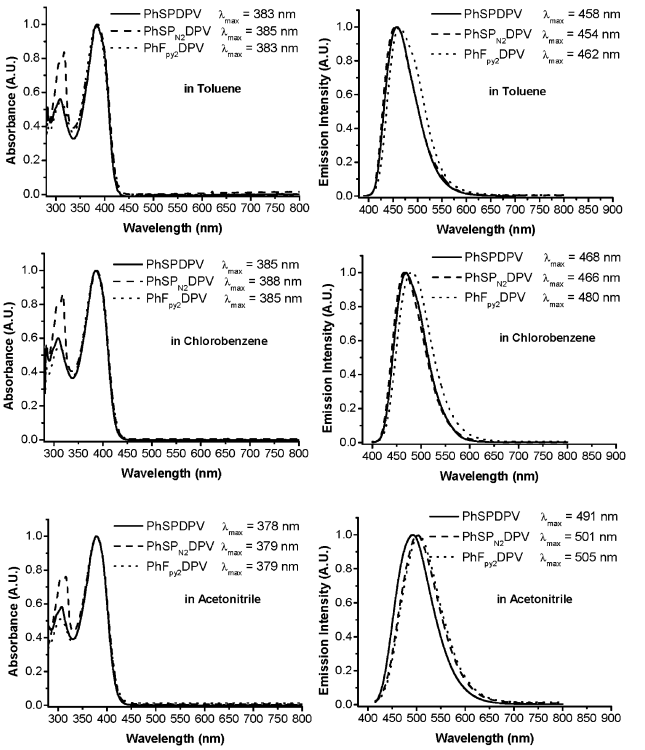

Fig. 3 Absorption (left) and emission (right) spectra of three blue emitters in three different solvents, toluene (top), chlorobenzene (center), and acetonitrile (bottom).

conceivable unless similar molecular structure (*i.e.*, 2-diphenylamino-7-diphenylvinylfluorene) constituting both HOMO and LUMO in all three fluorophores.

Unlike the lack of clear solvatochromism in absorption spectra, solvent polarity dependence is somewhat discernable in the emission spectra of **PhSPDPV**, **PhSP$_{N2}$DPV** and **PhF$_{py2}$DPV** (Fig. 3), although there lacks quantitative linear relationship in the plot of the fluorescence peak frequency as a function of solvent polarity. This indicates that the origin of the emission of the three blue emitters has limited character of intramolecular charge-transfer (ICT) or electron-transfer. Thus we can conclude that it is mainly non-directional π–π* transitions as the major feature in the emission of three blue emitters. However, considering the bathochromic emission in acetonitrile solution, we can not rule out that these blue fluorophores may adopt more polarized ICT state as the lowest excited state (involving LUMO +1 shown in Fig. 2 perhaps) under the influence of highly polar environment.

One should note that the magnitude of Stokes shift (the energy gap between the first absorption band and emission spectrum) is rather similar for **PhSPDPV** and **PhSP$_{N2}$DPV**. Stokes shift is 4274 and 3948 cm^{-1} in toluene, 4539 and 4314 cm^{-1} in chlorobenzene, and 6089 and 6425 cm^{-1} in acetonitrile, respectively for **PhSPDPV** and **PhSP$_{N2}$DPV**. From such results, we can derive that the dipole moment of the emission excited state of these two blue emitters should be rather similar. Once again, such derivation can not be justified unless the emission process does not involve 4,5-diazafluorene of **PhSP$_{N2}$DPV** or the unsubstituted fluorene moiety of **PhSPDPV**. Within this context, di(2,2′-pyridyl) substituent of **PhF$_{py2}$DPV** may be involved to a certain

extent in the emission process because of its larger Stokes shifts (4464, 5073, and 6584 cm^{-1} in toluene, chlorobenzene, and acetonitrile, respectively) when compared with those of **PhSPDPV** and **PhSP$_{N2}$DPV**. A lager Stokes shift indicates a higher degree of change about the electron density distribution between the ground state and lowest photoexcited state. The larger Stokes shifts also reflect in the emission energy of **PhF$_{py2}$DPV**, of which emission wavelength is always the longest among three blue emitters (Fig. 3).

PhSP$_{N2}$DPV has a relatively high fluorescence quantum yield (Φ_fs) of 66% in chlorobenzene (Table 1), which is slightly better than 60% of **PhSPDPV**. On the other hand, **PhF$_{py2}$DPV** has a significantly lower Φ_f of 48% in chlorobenzene, probable due to the vibrational quenching process of di(2,2′-pyridyl) substituent. Because of rotational vibration, di(2,2′-dipyridyl) moiety is relatively less rigid than fluorenyl of **PhSPDPV** or 4,5-diaza-fluorenyl of **PhSP$_{N2}$DPV**. In the solid state, three blue emitters all suffer from fluorescence concentration quenching, more or less resulting in a reduction of Φ_f (see data in Table 1). From solution to solid state, **PhSP$_{N2}$DPV** has the highest Φ_f reduction [(66 − 43)/66 = 35%] among three blue emitters and it can be attributed to its ground state dipole moment of ~4.4 Debye, which is relatively substantial when compared with virtually zero ground-state dipole moment (<1 Debye) of **PhSPDPV** or **PhF$_{py2}$DPV**. We have previously demonstrated that solid state fluorescence can be impaired by the molecular dipole.[10]

In order to probe the electron-accepting state of three blue emitters, electrochemical study was conducted by cyclic voltammetry (CV) and differential pulsed voltammetry (DPV). Due to the ill-profile of CV voltammograms, the redox potential values of three blue emitters were based on voltammograms of DPV (Fig. 4). As data listed in Table 1, the oxidation potential of three blue fluorophores was observed at a narrow potential range of +0.99 − +1.01 V *vs.* $Ag/AgNO_3$ (not shown in Fig. 4), which is common to most diphenylamine-substituted spirobifluorene compounds.[11] In the electrochemical measurement, we excluded the near constant reduction potential around -0.9 V because of the residual oxygen in electrolyte solution. We particularly pay attention to the electrochemical reduction potential of the three blue emitters because it is parallel to electron affinity. The electrochemical measurement recorded the first reduction potential of three blue fluorophores at −2.00 − −2.09 V *vs.* $Ag/AgNO_3$ (Fig. 4), which agrees quite well with the reduction potential of −2.00 V reported for 4,5-diaza-9,9′-spirobifluorene in tetrahydrofuran.[11a] Reduction potential is expected to be higher for **PhSPDPV** than **PhSP$_{N2}$DPV** or **PhF$_{py2}$DPV** due to the built-in electron deficient structure of the latter two fluorophores. According to the experimental data ($E_{1/2}^{red,1}$ or the energy level of LUMO derived from $E_{1/2}^{red,1}$) listed in Table 1, electron affinity is strongest for **PhSP$_{N2}$DPV**, followed by **PhF$_{py2}$DPV** and then **PhSPDPV**. Even though such order is the same as the energy levels of LUMO (Frank–Condon excited state) determined by spectroscopic method (Table 1), we tend to believe that the electron reduction (and hence electron transporting) happens *via* 4,5-diazafluorene of **PhSP$_{N2}$DPV** and di-2-pyridylmethylene of **PhF$_{py2}$DPV**, which is the molecular halve that is irrelevant to the emission process (luminescence).

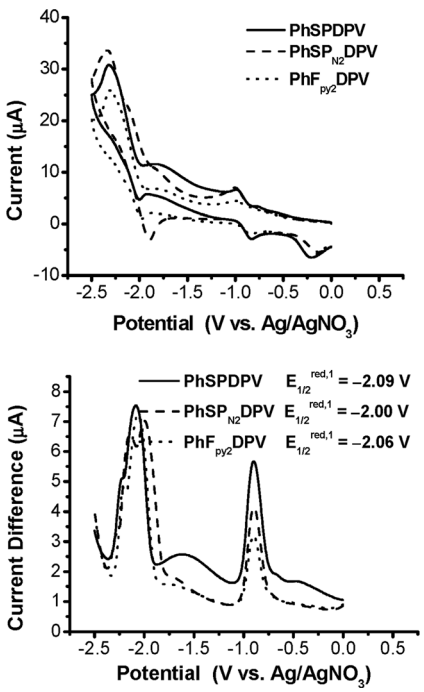

Fig. 4 Cyclic voltammograms (top) and differential pulsed voltammograms (bottom) of three blue emitters in tetrahydrofuran containing 0.1 M of $(Bu_4N)ClO_4$ as the supporting electrolyte.

Therefore, we seem to have two unusual cases (**PhSP$_{N2}$DPV** and **PhF$_{py2}$DPV**) that charge (electron) transporting and light-emitting primarily involve different molecular halves. 4,5-Diazafluorenyl or di(2,2′-diptridyl) molecular halve is responsible for charge-transporting and diphenylamino-diphenylvinyl-substituted molecular halve is the structural moiety that is luminescent. Such divider of the charge (electron)-transporting and light-emitting function has been identified before on 4,5-diazafluorene-incorporated ter(9,9′-di(*p*-tolyl)fluorene).[11a] However, we have found, for the first time, electrochemical reduction potentials (and hence electron affinity) of **PhSP$_{N2}$DPV** and **PhF$_{py2}$DPV** are closely related to their downward hole mobilities, instead of the electron mobilities (see following section for details). The new finding has profound influence on their OLED performance.

Charge carrier mobility and single-carrier devices

The charge-transporting characteristics of the blue emitters can be best understood by their charge carrier mobility *via* the transient photocurrent recorded by time-of-flight (TOF) method.[19] The field dependence of the charge carrier mobility of **PhSPDPV**, **PhSP$_{N2}$DPV**, and **PhF$_{py2}$DPV** is shown in Fig. 5. By extrapolating the data to the electric field at ~4.9×10^5 V cm^{-1} by the Poole–Frenkel relation, electron mobility is 8×10^{-4}, 5×10^{-5}, and 5×10^{-4} cm^2 V^{-1} s^{-1} for **PhSPDPV**, **PhSP$_{N2}$DPV**, and **PhF$_{py2}$DPV**, respectively. Apparently, the trend of electron mobility does not follow the order of electron affinity of three emitters. Electron deficient structure moiety does not necessary enhance the electron mobility. This is nothing to be surprised because electron mobility depends on internal reorganization energies for electron transfer, in addition to the electron affinity.[20] Furthermore, charge carrier mobility is highly

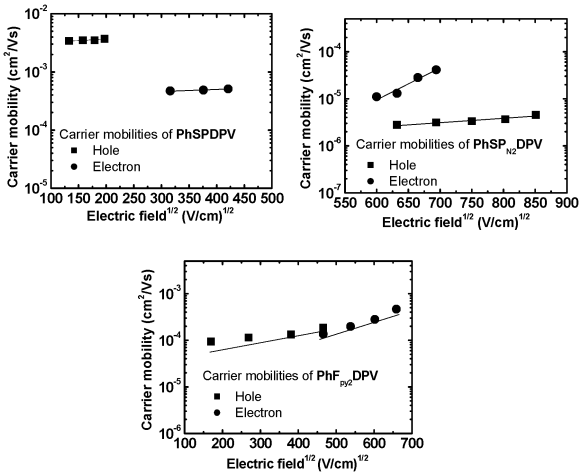

Fig. 5 Field dependent carrier mobilities of **PhSPDPV** (top left), **PhSP$_{N2}$DPV** (top right), and **PhF$_{py2}$DPV** (bottom).

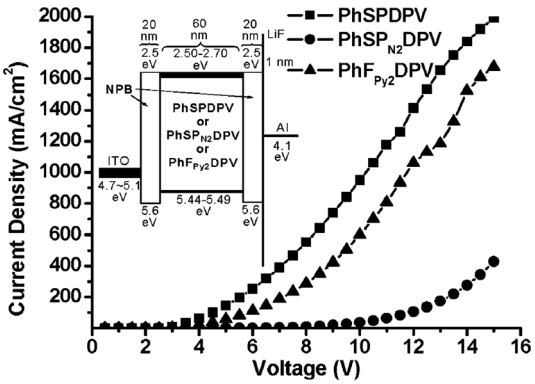

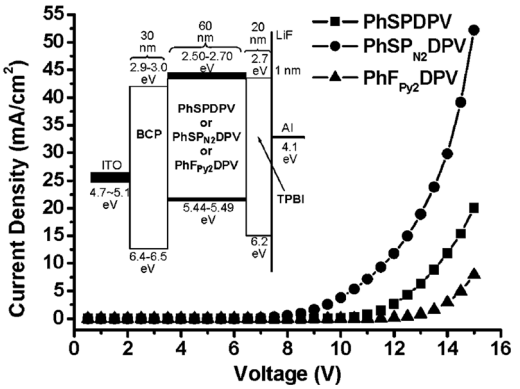

Fig. 6 Current density-voltage (I–V) characteristics of carrier-only devices: hole-only device (top) and electron-only device (bottom).

molecular interaction dependent, which is closely related to the molecular aggregation in solid state, *i.e.*, solid state order. Nevertheless, we do see the effect of those electron deficient moieties in lowering the hole mobility of the materials. Whereas the electron mobility of **PhSP$_{N2}$DPV** is still lower than that of **PhSPDPV**, at an electric field of 2.5×10^5 V cm^{-1} diaza substituent dramatically reduces the hole mobility from $\sim 6 \times 10^{-3}$ cm^2 V^{-1} s^{-1} of **PhSPDPV** down to $\sim 2 \times 10^{-6}$ cm^2 V^{-1} s^{-1} of **PhSP$_{N2}$DPV**. Similarly, a decreased hole mobility ($\sim 2 \times 10^{-4}$ cm^2 V^{-1} s^{-1} at $\sim 2.5 \times 10^5$ V cm^{-1}) was observed for **PhF$_{py2}$DPV**, although it is to a smaller extent when compared with that of **PhSP$_{N2}$DPV**. Interestingly, for **PhSP$_{N2}$DPV** and **PhF$_{py2}$DPV**, the decrease of the hole mobility is parallel to the increase of the electron affinity.

We also fabricated the single-carrier devices for the evaluation of the charge carrier mobility in terms of current density of **PhSPDPV**, **PhSP$_{N2}$DPV**, and **PhF$_{py2}$DPV**. As shown in the inset of Fig. 6, we used high-LUMO NPB to limit the electron carrier in hole-only devices and low-HOMO BCP (2,9-dimethyl-4,7-diphenyl-1,10-phenanthroline) and TPBI (2,2′,2″-(1,2,5-phenylene)tris(1-phenyl-1*H*-benzimidazole) to limit the hole carrier in electron-only devices. For the hole-only devices, the magnitude of current density clearly follows the order of hole mobility of three blue emitters, which is **PhSPDPV** > **PhF$_{py2}$DPV** > **PhSP$_{N2}$DPV**. One should note that the current density of a hole-only device is determined by several factors, hole injection barrier between the electrode and organic layer, the difference of the HOMO energy levels between the adjacent organic layers, and the hole mobility of each organic layers. In the case studied herein, HOMO energy levels of three blue emitters are relatively invariant, the biggest difference among blue emitters is only 0.05 eV. Therefore, the hole mobility of the blue emitters becomes the sole factor in determining current density of the hole-only devices. The situation of the current density of electron-only devices is more complicated. First, it is highly possible that the molecular part of the molecule involving electron transporting of **PhSPDPV** is different from that of **PhF$_{py2}$DPV** or **PhSP$_{N2}$DPV**. Second, the variation of LUMO energy levels of the three blue emitters is not negligible and the variation can be as high as 0.15 eV. According to the estimated LUMO energy levels, **PhSP$_{N2}$DPV** has the lowest LUMO energy level and it is the nearest one to the LUMO energy level of BCP or TPBI. Therefore, among three blue emitters, it is **PhSP$_{N2}$DPV** to show highest current density in electron-only device, even though its electron mobility is not the highest among three blue emitters. On the other hand, **PhF$_{py2}$DPV** shows lower current density than does **PhSPDPV** and it can be attributed to its lower electron mobility. However, such current density analysis of electron-only devices seems to be over simplified. For hole-only device, NPB has a hole mobility of $\sim 5.5 \times 10^{-3}$ cm^2 V^{-1} s^{-1},[21] which is comparable with that of **PhSPDPV** and significantly higher than that of **PhSP$_{N2}$DPV** or **PhSP$_{py2}$DPV**. This is not quite the same for electron-only devices. Unlike three blue fluorophores dominating the current density in hole-only devices, it is BCP or TPBI instead of blue emitters as the limiting factor of the current density in electron-only devices. Literature reported value of the electron mobility is about 5×10^{-7} and 5×10^{-6} cm^2 V^{-1} s^{-1} (at an electric field of $\sim 4.9 \times 10^5$ V cm^{-1}) for BCP and TPBI, respectively.[22] This further complicates the assessment of the electron mobility *via* the current density of electron-only device.

OLED characterization

Table 2 and Fig. 7 summarize the EL characteristics of three non-doped OLEDs based on three blue emitters studied herein. For

Table 2 Electroluminescence characteristics of non-doped blue OLEDs of **PhSPDPV**, **PhSP$_{N2}$DPV**, and **PhF$_{Py2}$DPV**[a]

	Max. luminance and voltage (cd m^{-2}, V)	Luminance, Efficiency, Voltage (cd m^{-2}, %, V)[b]	Max. Efficiency (%, cd A^{-1}, lm W^{-1})	λ_{max}^{el} (nm)	1931 CIE Chromaticity (x, y)
PhSPDPV	33020, 15	910, 2.9, 4.7	3.4, 5.4, 5.7	478	0.14, 0.22
PhSP$_{N2}$DPV	60510, 15	1810, 4.4, 5.2	4.9, 10.2, 10.5	488	0.16, 0.32
PhF$_{Py2}$DPV	15070, 15	1140, 2.8, 5.1	3.2, 6.4, 5.7	486	0.15, 0.31

[a] Devices have the configuration of ITO/NPB (10 nm)/blue emitter (40 nm)/TPBI (50 nm)/LiF (1 nm)/Al (150 nm). [b] At current density of 20 mA cm^{-2}.

a fair comparison, three non-doped OLEDs have a same simple three-layer configuration: ITO/NPB (10 nm)/blue emitter (40 nm)/TPBI (50 nm)/LiF (1 nm)/Al (150 nm), where NPB is a common hole transporting layer, TPBI is a common electron transporting layer. No exotic or fancy hole/electron-injecting layer or hole-blocking layer is necessary herein. Whereas **PhF$_{py2}$DPV** OLED is slightly better than **PhSPDPV** one, bipolar emitter **PhSP$_{N2}$DPV** significantly outperforms previously known **PhSPDPV**. **PhSP$_{N2}$DPV** OLED has a remarkable EL performance: maximum efficiency of ~5% (or ~10 ml W^{-1}), peak brightness of 60,000 cd m^{-2} (~1,800 cd m^{-2} at 20 mA cm^{-2}). More significantly, within a range of brightness (100 ~ 1,000 cd m^{-2}) required for SSL, **PhSP$_{N2}$DPV** exhibits only miner efficiency roll-off from 1 to 20 mA cm^{-2} with η_{EXT} of ~5.0% to 4.6%. Such performance ranks **PhSP$_{N2}$DPV** on top of most electrofluorescence-based blue OLEDs and rivals those super-efficient ones.[7] However, compared with thin-film emission peak wavelength (Table 1), 6–11 nm of red-shifting were observed for EL of three blue emitters. Whereas **PhSPDPV** OLED is blue CIE$_{x,y}$ = 0.14, 0.22, **PhSP$_{N2}$DPV** and **PhF$_{py2}$DPV** OLEDs exhibit sky blue color CIE$_{x,y}$ = 0.16, 0.32 and CIE$_{x,y}$ = 0.15, 0.31, respectively (Fig. 7a). In most cases, a sky blue OLED often performs better than a true blue OLED. However, high-performance **PhSP$_{N2}$DPV** OLED is not simply a matter of color purity because the performance of similarly sky blue **PhF$_{py2}$DPV** OLED is not much better than that of **PhSPDPV** OLED (Table 2). Moreover, **PhSP$_{N2}$DPV** has Φ_f around 43% in the solid state, which is substantially lower than Φ_f 51% of **PhSPDPV** but very similar to 42% of **PhF$_{py2}$DPV**.

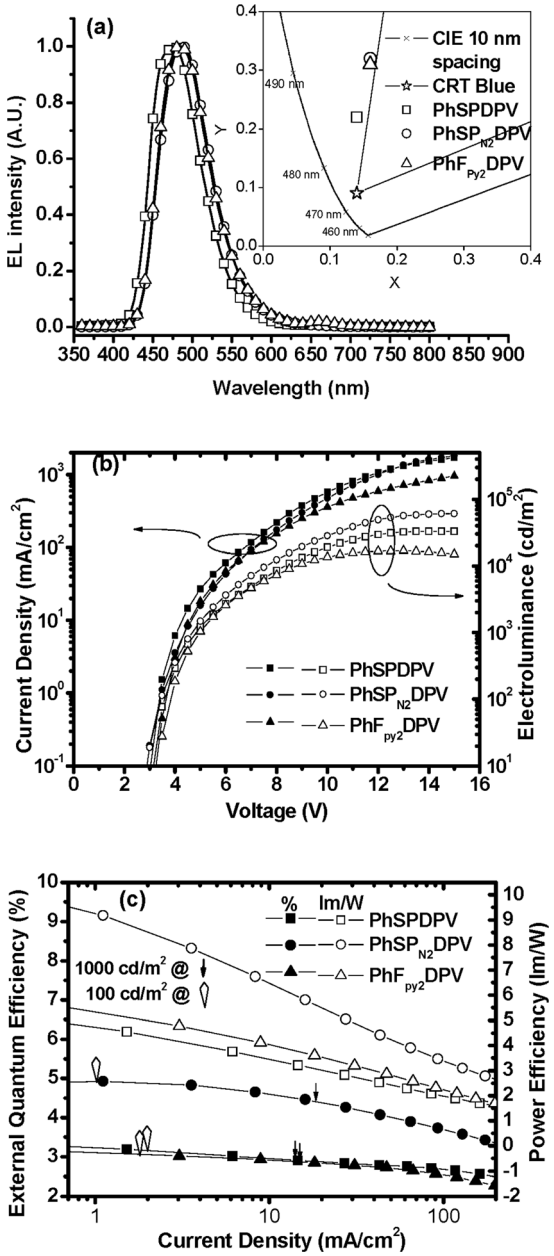

Fig. 7 Electroluminescence (EL) characteristics of non-doped blue OLEDs: **PhSPDPV**, **PhSP$_{N2}$DPV**, and **PhF$_{py2}$PV**. EL spectra and CIE chromaticity diagram (a), *J*–*V*–*L* (b), and η_{EXT}–*J*–η_{PW} (c) characteristics of devices.

The superior performance of **PhSP$_{N2}$DPV** OLED compared with **PhSPDPV** or **PhF$_{py2}$DPV** OLED can be mainly attributed to the issue of charge balancing in their OLEDs. **PhSPDPV** behaves like a typical π-conjugated organic material: hole mobility is an order of magnitude higher than electron mobility. This is quite different from the electron deficient **PhF$_{py2}$DPV** or **PhSP$_{N2}$DPV**. Whereas **PhF$_{py2}$DPV** seems to be ambipolar (hole and electron nobilities are quite similar to each other around 5 × 10^{-4} cm^2 V^{-1} s^{-1} at an electric field of ~4.9 × 10^5 V cm^{-1}), **PhSP$_{N2}$DPV** has a very low hole mobility of 3 × 10^{-6} cm^2 V^{-1} s^{-1}, which is even lower than its electron mobility 5 × 10^{-5} cm^2 V^{-1} s^{-1} at the same electric field (Fig. 5). With such characteristics in charge carrier mobility (a significantly reduced hole mobility), **PhSP$_{N2}$DPV** OLED can be expected to be superb in EL efficiency (maximum η_{EXT} ~5% and 4.6% at 20 mA cm^{-2}) because of the satisfactory situation of charge balancing. Normally, an excess amount of hole carrier is expected if **PhSP$_{N2}$DPV** (or **PhF$_{py2}$DPV**) is absent in the device, *i.e.*, ITO/NPB/TPBI/LiF/Al is a hole-excess device. Within this context, charge balancing is not optimized in **PhSPDPV** OLED and its EL efficiency is expected to be less satisfactory because of very high hole mobility (5 × 10^{-3} cm^2 V^{-1} s^{-1} at an electric field of ~2.5 × 10^5 V cm^{-1}) and relatively low electron mobility (5 × 10^{-4} cm^2 V^{-1} s^{-1} at an

electric field of $\sim 2.5 \times 10^5$ V cm^{-1}) (see Fig. 5). However, it is the relatively high Φ_f (51%) of **PhSPDPV** in the solid state rendering η_{EXT} (maximum 3.4% and 2.9% at 20 mA cm^{-2}) to be comparable with or slightly better than that (η_{EXT} maximum 3.2% and 2.8% at 20 mA cm^{-2}) of **PhF$_{py2}$DPV** OLED.

Conclusions

In this study, we have synthesized and characterized two unusual bipolar fluorophores, **PhSP$_{N2}$DPV** and **PhF$_{py2}$DPV**, which exhibit high performance when applied for OLEDs. Particularly, non-doped **PhSP$_{N2}$DPV** OLED display sky-blue EL very bright (peak intensity of 60510 cd m^{-2} or 1810 cd m^{-2} at 20 mA cm^{-2}) and efficient (maximum external quantum efficiency 4.9% or 4.4% at 20 mA cm^{-2}), having minimum efficiency roll-off, 4.9% at 100 cd cm^{-2} ($\sim$1 mA cm^{-2}) and 4.6% at 1,000 cd cm^{-2} ($\sim$19 mA cm^{-2}). **PhSP$_{N2}$DPV** with such EL performance rivals those super-efficient electrofluorescence blue OLEDs and is potential alternative for troublesome electrophosphorescence blue OLEDs. Fundamentally, we have demonstrated that the reduction of the hole mobility is crucial for charge balancing in high efficiency OLEDs. Moreover, we have verified that both **PhSP$_{N2}$DPV** and **PhF$_{py2}$DPV** have one molecular halve responsible for electron-transporting and the other molecular halve for light-emitting. Such a structural separation in charge-transporting and light-emitting processes renders a potent molecular design in the optimization of fluorescent materials for EL application.

Experimental

General methods

Both solution and solid-state fluorescence quantum yields (Φ_fs) of the blue emitters were determined by the integrating-sphere method.[23] The ionization potentials (or HOMO energy levels) of three compounds were determined by low energy photo-electron spectrometer (Riken-Keiki AC-2). From our previous data, we found that the precision of AC-2 measurement is about $\pm$0.05 eV. LUMO energy levels were estimated by subtracting the energy gap (ΔE) from HOMO energy levels. ΔE was determined by the on-set absorption energy from the absorption spectra of the materials as thin films. UV-visible electronic absorption spectra were recorded on a Hewlett-Packard 8453 Diode Array Spectrophotometer. Cyclic voltammetry (CV) and differential pulsed voltammetry (DPV) were performed using an Electrochemical Analyzer BAS C3. The measurement, using a glassy carbon rod as the working electrode and a platinum wire as the counter electrode, was performed in a 0.1 M solution of $(Bu_4N)ClO_4$ in anhydrous tetrahydrofuran. The reported redox potentials were estimated from DPV voltammograms in volts *vs* saturated $Ag/AgNO_3$ reference potential. We used ferrocene/ferrocenium (0.63 V *vs* $Ag/AgNO_3$) as reversibility criteria and the calibration for energy levels (4.8 eV below the vacuum level).[18] The method of time-of-flight (TOF) in measuring charge carrier mobility has been described before.[19]

Synthesis of materials

4,5-Diaza-2′,7′-dibromo-9,9′-spirobifluorene was prepared according to a procedure previously reported by Wong *et al.*[11] 2-Amino-4,4′-dibromobiphenyl was prepared in two steps from 4,4′-dibromobiphenyl according to published procedures.[12] For the materials used in device fabrication, BCP (2,9-dimethyl-4,7-diphenyl-1,10-phenanthroline) was commercially available material. NPB (4,4′-bis[*N*-(1-naphthyl)-*N*-phenylamino]-biphenyl)[24a] and TPBI (2,2′,2″-(1,2,5-phenylene)-tris(1-phenyl-1H-benzimidazole)[24b] were prepared *via* published methods and were subjected to gradient sublimation prior to use.

4,5-Diaza-2′-bromo-9,9′-spirobifluorene-7′-carboxaldehyde. To a THF solution (650 mL) of 4,5-diaza-2′,7′-dibromo-9,9′-spirobifluorene (4.76 g, 10.0 mmol) was added *n*-BuLi (4.8 mL, 12.0 mmol, 1.6 M in hexane) slowly at -78 °C. The mixture was stirred for 1 h under nitrogen atmosphere. After the slow addition of DMF (2.33 mL, 30.0 mmol), the reaction solution was gradually warmed up to room temperature and kept at this temperature overnight. The reaction was quenched with a 2 N HCl aqueous solution, extracted with ethyl acetate, and dried over $MgSO_4$. The solution was concentrated under reduced pressure and subjected to flash column chromatography (silica gel, ethyl acetate/toluene: 2/3). A white solid was obtained with a yield of 40% (1.7 g). ^{1}H NMR (400 MHz, $CDCl_3$): δ 9.80 (s, 1H), 8.77 (dd, 2H, J = 4.6, 1.6 Hz), 7.97 (d, 1H, J = 7.8 Hz), 7.94 (dd, 1H, J = 7.9, 1.3 Hz), 7.79 (d, 1H, J = 8.2 Hz), 7.58 (dd, 1H, J = 8.2, 1.8 Hz), 7.22 (d, 1H, J = 1.3 Hz), 7.16 (d, 1H, J = 4.8 Hz), 7.14 (d, 1H, J = 4.7 Hz), 7.10 (dd, 2H, J = 7.7, 1.6 Hz), 6.89 (d, 1H, J = 1.7 Hz). ^{13}C NMR (100 MHz, $CDCl_3$): δ 190.1, 158.8, 150.8, 149.2, 146.7, 146.5, 141.8, 139.1, 136.4, 132.1, 131.6, 130.9, 127.3, 124.8, 123.8, 123.7, 122.7, 120.8, 61.1. FAB-MS: calcd. 424.02, m/z = 425.03/427.03 (M + H$^+$).

4,5-Diaza-2′-diphenylamino-9,9′-spirobifluorene-7′-carboxaldehyde. A mixture of 4,5-diaza-2′-bromo-9,9′-spirobifluorene-7′-carboxaldehyde (1.47 g, 3.45 mmol), diphenylamine (0.64 g, 3.8 mmol), $Pd(OAc)_2$ (70 mg, 0.3 mmol), Cs_2CO_3 (1.24 g, 3.8 mmol), and P(tBu)$_3$ (0.12 g, 0.6 mmol) in toluene (35 mL) was stirred at 120 °C for 6 h under nitrogen atmosphere. After cooling to room temperature, a saturated ammonium chloride solution was added to the reaction solution. The solution was extracted with dichloromethane and dried over $MgSO_4$. The solution was concentrated under reduced pressure and subjected to flash column chromatography (silica gel, ethyl acetate/hexanes: 3/2). A yellow solid was obtained with a yield of 55% (0.98 g). ^{1}H NMR (400 MHz, $CDCl_3$): δ 9.77 (s, 1H), 8.70 (dd, 2H, J = 4.6, 1.7 Hz), 7.89 (dd, 1H, J = 7.9, 1.4 Hz), 7.84 (d, 1H, J = 7.9 Hz), 7.10–7.20 (m, 9H), 7.74 (d, 1H, J = 8.4 Hz), 7.05 (dd, 1H, J = 8.4, 2.1 Hz), 6.90–6.98 (m, 6H), 6.42 (d, 1H, J = 2.0 Hz). ^{13}C NMR (100 MHz, $CDCl_3$): δ 191.2, 158.9, 150.6, 149.8, 149.0, 147.9, 146.8, 142.7, 135.2, 133.7, 131.6, 129.3, 131.1, 124.7, 123.9, 123.7, 122.9, 122.2, 119.7, 117.4, 61.2. FAB-MS: calcd. 513.18, m/z = 514.19 (M + H$^+$).

4,5-Diaza-2′-diphenylamino-7′-(2,2″-diphenylvinyl)-9,9′-spirobifluorene (PhSP$_{N2}$DPV). To diethoxydiphenylmethylphosphonate (6.8 g, 22.0 mmol) in dry THF (10 mL) was added NaH (0.96 g, 60% w/w dispersion in mineral oil, 24.0 mmol), and stirred for 1 h at 55 °C under nitrogen atmosphere. After cooling to room temperature, 4,5-diaza-2′-diphenylamino-9,9′-spirobifluorene-7′-carboxaldehyde (1.21 g, 2.36 mmol) was added, the reaction

solution was heated at reflux temperature overnight. After cooling to room temperature, the reaction mixture was added to water, extracted with ethyl acetate, and dried over $MgSO_4$. The solution was concentrated under reduced pressure and subjected to flash column chromatography (silica gel, ethyl acetate/hexanes: 2/3). A yellow solid was obtained with a yield of 68% (1.06 g). ^{1}H NMR (400 MHz, $CDCl_3$): δ 8.65 (dd, 2H, $J = 4.4$, 1.9 Hz), 7.57 (d, 1H, $J = 8.3$ Hz), 7.54 (d, 1H, $J = 7.9$ Hz), 7.16–7.23 (m, 5H), 7.07–7.16 (m, 9H), 6.96–7.07 (m, 4H), 6.86–6.96 (m, 8H), 6.82 (s, 1H), 6.34 (d, 1H, $J = 2.0$ Hz), 5.94 (s, 1H). ^{13}C NMR (100 MHz, $CDCl_3$): δ 158.6, 150.0, 148.0, 147.7, 147.2, 145.6, 143.3, 142.6 (×2), 140.1, 139.7, 136.5, 135.8, 131.5, 130.4, 129.6 (×2), 129.1, 128.4, 128.1, 127.5, 127.4, 127.2, 124.2, 124.1, 123.6, 123.5, 123.1, 120.8, 119.1, 118.7, 61.1. FAB-MS: calcd. 663.27, $m/z = 664.27$ ($M + H^+$). Anal. calcd for $C_{49}H_{33}N_3$: C 88.66, H 5.01, N 6.33; found: C 88.49, H 5.14, N 6.23.

2-Iodo-4,4′-dibromobiphenyl. A solution of sodium nitrite (1.16 g, 16.8 mmol) in water (5 mL) was added dropwise at 0 °C to a mixture of 2-amino-4,4′-dibromobiphenyl (5.0 g, 15.3 mmol) and 8 N HCl aqueous solution (100 mL). After 30 min of stirring, an aqueous solution of potassium iodide (2.8 g, 16.8 mmol) was added during 5 min and the mixture was warmed up to room temperature for 1 h. The solution was extracted with diethyl ether. The organic phase was washed with an aqueous solution of $NaHSO_3$ and water, and dried over $MgSO_4$. The solution was concentrated under reduced pressure and subjected to flash column chromatography (silica gel, hexanes). A white solid was obtained with a yield of 67% (4.5 g). ^{1}H NMR (400 MHz, $CDCl_3$): δ 8.08 (d, 1H, $J = 2.0$ Hz), 7.53 (dm, 2H, $J = 8.5$ Hz), 7.16 (dm, 2H, $J = 8.5$ Hz), 7.11 (d, 1H, $J = 8.2$ Hz). ^{13}C NMR (100 MHz, $CDCl_3$): δ 144.4, 141.9, 141.5, 131.4, 131.3, 130.8, 130.7, 122.3, 121.9, 98.7. EI-MS: calcd. 435.8, m/z 435.8/437.9 (M^+).

2-[Di(2,2″-pyridyl)hydroxymethyl]-4,4′-dibromobiphenyl. To a THF solution (100 mL) of 2-iodo-4,4′-dibromodiphenyl (10.0 g, 23 mmol) was added *n*-BuLi (15.6 mL, 25 mmol, 1.6 M in hexane) slowly at −78 °C. The mixture was stirred for 1 h under nitrogen atmosphere. Di(2-pyridyl) ketone (4.6 g, 9.3 mmol) in THF (20 mL) was added to the reaction solution at −78 °C. The mixture was continuously stirred at −78 °C for 1 h and then warmed up to room temperature for 1 h. Saturated ammonium chloride solution was added to the reaction solution. The solution was extracted with ethyl acetate and dried over $MgSO_4$. The solution was concentrated under reduced pressure and subjected to flash column chromatography (silica gel, ethyl acetate/hexanes: 1/10). A white solid was obtained with a yield of 86% (9.7 g). ^{1}H NMR (400 MHz, $CDCl_3$): δ 8.39 (m, 2H), 7.61 (d, 2H, $J = 8.0$ Hz), 7.49 (td, 2H, J = 7.8, 1.7 Hz), 7.39 (dd, 1H, $J = 8.1$, 2.0 Hz), 7.10–7.05 (m, 5H), 6.93 (d, 1H, $J = 8.1$ Hz), 6.88 (d, 1H, $J = 2.0$ Hz), 6.82 (d, 2H, $J = 8.4$ Hz). ^{13}C NMR (100 MHz, $CDCl_3$): δ 162.1, 147.1, 147.0, 141.1, 140.4, 136.3, 133.6, 131.8 (×2), 130.3, 129.5, 123.0, 122.2, 121.1, 120.3, 80.5. FAB-MS: calcd. 494.0, $m/z = 495.0/497.0$ ($M + H^+$). Anal. calcd for $C_{23}H_{16}Br_2N_2O$: C 55.67, H 3.25, N 5.65; found: C 55.67, H 3.13, N 5.70.

2-[Di(2,2″-pyridyl)chloromethyl]-4,4′-dibromobiphenyl. The functional group transformation from carbinol to chloride was performed by pertinent literature method.[25] To the carbinol (4.5 g, 9.18 mmol) in dry THF (50 mL) was added NaH (0.48 g, 60% w/w dispersion in mineral oil, 12 mmol) and stirred for 1 h at room temperature. After cooling the reaction solution to 0 °C, thionyl chloride (0.9 mL, 12 mmol) was added dropwise to the mixture and stirred for 1 h. The reaction was quenched with saturated $NaHCO_3$ solution, extracted with dichloromethane and dried over Na_2SO_4. The solution was concentrated under reduced pressure. Chloro-substituted product was obtained as a pale yellow solid. It was used directly in the next step of synthesis without further purification. ^{1}H NMR (400 MHz, $CDCl_3$): δ 8.5 (d, 2H, $J = 4.4$ Hz), 7.52–7.40 (m, 6H), 7.10 (dd, 2H, $J = 7.3$, 4.8 Hz), 7.01 (d, 2H, $J = 8.4$ Hz), 6.90 (d, 1H, $J = 8.0$ Hz), 6.66 (d, 2H, $J = 8.3$ Hz).

2,7-Dibromo-9,9′-di(2,2″-pyridyl)fluorene. The crude chloro-substituted intermediate was dissolved in nitromethane (50 mL). Powdered aluminium chloride (5.0 g, 37 mmol) was added to the solution at room temperature under nitrogen atmosphere and then heated under reflux for overnight. After cooling to room temperature, saturated $NaHCO_3$ solution was carefully added to the reaction mixture and then extracted with dichloromethane for several times. The organic solution was concentrated under reduced pressure and a large amount diethyl ether was poured into the residue. A light yellow solid was obtained after filtration. The filtrate was purified from flash column chromatography (silica gel, ethyl acetate/hexanes: 1/4) and a white solid was obtained. In combining two solid samples, 2,7-dibromo-9,9′-di(2,2″-pyridyl)fluorene was obtained with a yield of 75% (3.3 g). ^{1}H NMR (400 MHz, $CDCl_3$): δ 8.62–8.57 (m, 2H), 7.95 (d, 2H, $J = 1.7$ Hz), 7.59 (d, 2H, $J = 8.1$ Hz), 7.55–7.47 (m, 4H), 7.15–7.10 (m, 2H), 7.0 (d, 2H, $J = 8.0$ Hz). ^{13}C NMR (100 MHz, $CDCl_3$): δ 162.9, 150.0, 149.8, 138.7, 136.6, 131.4, 130.4, 122.0, 121.8, 121.5, 120.9, 68.8. EI-MS: calcd. 476.0, $m/z = 476.0/478.0$ (M^+). Anal. calcd for $C_{23}H_{14}Br_2N_2$: C 57.77, H 2.95, N 5.86; found: C 57.34, H 2.81, N 5.90.

7-Bromo-9,9′-di(2,2″-pyridyl)-2-fluorenecarboxaldehyde. This compound was prepared similarly to that of 4,5-diaza-2′-bromo-9,9′-spirobifluorene-7′-carboxaldehyde, except that 2,7-dibromo-9,9′-di(2,2″-pyridyl)fluorene (2.0 g, 4.18 mmol) was used in the reaction, and ethyl acetate/dichloromethane/hexanes (1/1/2) was used as eluent for flash column chromatography. A milk-white solid was obtained with a yield of 58% (1.03 g). ^{1}H NMR (400 MHz, $CDCl_3$): δ 9.99 (s, 1H), 8.62–8.57 (m, 2H), 8.29 (d, 1H, $J = 0.8$ Hz), 8.01 (d, 1H, $J = 1.7$ Hz), 7.95 (dd, 1H, $J = 7.9$, 1.4 Hz), 7.87 (d, 1H, $J = 7.9$ Hz), 7.70 (d, 1H, $J = 8.1$ Hz), 7.57 (dd, 1H, $J = 8.2$, 1.8 Hz), 7.51 (td, 2H, $J = 7.8$, 1.9 Hz), 7.13 (ddd, 2H, $J = 7.5$, 4.8, 1.0 Hz), 7.01 (d, 2H, $J = 7.2$ Hz). ^{13}C NMR (100 MHz, $CDCl_3$): δ 191.8, 162.6, 151.4, 150.0, 148.7, 145.8, 138.3, 136.6, 136.2, 131.7, 130.7, 129.8, 129.2, 123.3, 122.5, 122.1, 120.7, 68.8. FAB-MS: calcd. 426.0, $m/z = 427.1$ ($M + H^+$).

7-(Diphenylamino)-9,9′-di(2,2″-pyridyl)-2-fluorenecarboxaldehyde. A mixture of 7-bromo-9,9′-di(2,2″-pyridyl)-2-fluorenecarboxaldehyde (1.92 g, 4.5 mmol), diphenylamine (1.14 g, 6.75 mmol), $Pd(OAc)_2$ (25 mg, 0.113 mmol), $P(tBu)_3$ (47 mg, 0.23 mmol), and Cs_2CO_3 (3.3 g, 10.1 mmol) in toluene (300 mL) was reacted in a similar fashion to that of preparing 4,5-diaza-2′-diphenylamino-9,9′-spirobifluorene-7′-carboxaldehyde, except

the reaction time was extended to 3 days, and ethyl acetate/dichloromethane (1/4) was used as the eluent for flash column chromatography. A yellow solid was obtained with a yield of 77% (1.78 g). ^{1}H NMR (400 MHz, $CDCl_3$): δ 9.95 (s, 1H), 8.53–8.50 (m, 2H), 7.24 (d, 1H, $J = 1.0$ Hz), 7.91 (dd, 1H, $J = 7.9$, 1.4 Hz), 7.77 (d, 1H, $J = 7.9$ Hz), 7.65 (d, 1H, J = 8.4 Hz), 7.57 (d, 1H, J = 1.8 Hz), 7.48 (td, 2H, $J = 7.8$, 1.9 Hz), 7.23–7.17 (m, 4H), 7.12–6.98 (m, 11H). ^{13}C NMR (100 MHz, $CDCl_3$): δ 191.9, 163.2, 151.0, 149.8, 149.2, 148.6, 147.3, 146.9, 136.4, 135.0, 133.0, 129.8, 129.3, 129.2, 124.7, 123.4, 123.0, 121.9, 121.8 (×2), 121.0, 119.7, 68.6. FAB-MS: calcd. 515.6, $m/z = 516.2$ (M + H$^+$).

***N*-[7-(2,2-Diphenylvinyl)-9,9′-di(2,2″-pyridyl)-2-fluorenyl]-*N*,*N*-diphenylamine ($PhF_{py2}DPV$).** A mixture of 7-(diphenylamino)-9,9′-di(2,2″-pyridyl)-2-fluorenecarboxaldehyde (0.92 g, 1.6 mmol), diethoxydiphenylmethylphosphonate (1.95 g, 6.4 mmol), and NaH (0.28 g, 60% w/w dispersion in mineral oil, 7.0 mmol) in dry THF (40 mL) was reacted in a similar fashion to that of preparing 4,5-diaza-2′-diphenylamino-7′-(2,2′-diphenylvinyl)-9,9′-spirobifluorene, except the reaction time was extended to overnight, and ethyl acetate/hexanes (1/4) was used as the eluent for flash column chromatography. The remaining diethoxydiphenylmethylphosphonate can be removed after sublimination. A yellow-green solid was obtained with a yield of 67% (0.71g). ^{1}H NMR (400 MHz, $CDCl_3$): δ 8.43 (dd, 2H, $J = 4.7$, 0.8 Hz), 7.59 (d, 1H, $J = 1.3$ Hz), 7.50 (d, 1H, $J = 8.2$ Hz), 7.47–7.40 (m, 4H), 7.30–7.20 (m, 8H), 7.19–7.13 (m, 6H), 7.06–6.98 (m, 9H), 6.94 (t, 2H, $J = 7.3$ Hz), 6.87 (d, 2H, $J = 8.0$ Hz). ^{13}C NMR (100 MHz, CDCl3): δ 163.8, 150.1, 149.5, 147.7, 147.6, 147.5, 143.5, 142.1, 140.4, 139.3, 136.3, 136.1, 134.9, 130.5, 129.3, 129.1, 128.7, 128.5 (×2), 128.1, 127.5, 127.4, 127.3, 124.1, 123.7, 123.1, 122.7, 121.4, 121.0, 120.4, 119.1, 68.6. FAB-MS: calcd. 665.3, $m/z = 666.2$ (M + H$^+$). Anal. calcd for $C_{49}H_{35}N_3$: C 88.39, H 5.30, N 6.31; found: C 88.13, H 5.40, N 6.01.

X-Ray crystallography studies†

Data collection was carried out on a Brucker X8APEX CCD diffractometer at 100 K for **$PhSP_{N2}DPV$** and **$PhF_{py2}DPV$** single crystals. The radiation of Mo radiation (λ = 0.71073 Å) was used for both crystals. The unit cell parameters were obtained by a least-square fit to the automatically centered settings for reflections. Intensity data were collected by using the $\omega/2\theta$ scan mode. Corrections were made for Lorentz and polarization effects. The structures were solved by direct methods *SHELX-97*.[26] All non-hydrogen atoms were located from the difference Fourier maps and were refined by full-matrix least-squares procedures. The position of hydrogen atoms was calculated and located. Calculations and full-matrix least-squares refinements were performed utilizing the *WINGX* program package[27] in the evaluation of values of R (F_o) for reflections with I > 2σ(I) and R_w (F_o), where $R = \Sigma||F_o| - |F_c||/\Sigma|F_o|$ and $R_w = [\Sigma\{w(F_o^2 - F_c^2)^2\}/\Sigma\{w(F_o^2)^2\}]^{1/2}$. Intensities were corrected for absorption.

OLED fabrication and electroluminescence (EL) characterization

The fabrication of OLEDs and their EL characterization have been described elsewhere.[28] The current density-voltage-light intensity (*J–V–L*) measurements were made simultaneously using a Keithley 2400 programmable source meter and a Newport 1835C Optical meter equipped with a Newport 818-ST silicon photodiode. The device was placed close to the photodiode such that all the forward light went to the photodiode. The effective size of the emitting diode was 3.14 mm^2, which is significantly smaller than the active area of the photodiode detector, a condition known as "under filling" to satisfy the measurement protocol.[29] Only light emitting from the front face of the devices was collected and used in subsequent calculations of external quantum efficiency (η_{EXT}) according to the method described earlier.[29] The luminous flux (lm) has been defined previously,[30] and we adopted it to estimate the power efficiency (η_P) of OLEDs.

Acknowledgements

This research was supported in part by the National Science Council of Taiwan, National Chiao Tung University, and Academia Sinica. The authors also thank Prof. Chao-Ping Hsu for helpful instruction and discussion in theoretical calculation.

References

1 (*a*) A. Köhler, J. S. Wilson and R. H. Friend, *Adv. Mater.*, 2002, **14**, 701; (*b*) S. R. Forrest, *Org. Electron.*, 2003, **4**, 45.
2 (*a*) Y. Sun, N. C. Giebink, H. Kanno, B. Ma, M. E. Thompson and S. R. Forrest, *Nature*, 2006, **440**, 908; (*b*) P.-I. Shih, C.-F. Shu, Y.-L. Tung and Y. Chi, *Appl. Phys. Lett.*, 2006, **88**, 251110; (*c*) G. Schwartz, K. Fehse, M. Pfeiffer, K. Walzer and K. Leo, *Appl. Phys. Lett.*, 2006, **89**, 083509; (*d*) H. Kanno, Y. Sun and S. R. Forrest, *Appl. Phys. Lett.*, 2006, **89**, 143516; (*e*) B.-P. Yan, C. C. C. Cheung, S. C. F. Kui, H.-F. Xiang, V. A. L. Roy, S.-J. Xu and C.-M. Che, *Adv. Mater.*, 2007, **19**, 3599; (*f*) G. Schwartz, M. Pfeiffer, S. Reineke, K. Walzer and K. Leo, *Adv. Mater.*, 2007, **19**, 3672.
3 (*a*) A. B. Chwang, M. Hack and J. L. Brown, *J. Soc. Inform. Display*, 2005, **13**, 481; (*b*) M. S. Weaver, R. C. Kwong, V. A. Adamovic, M. Kack and J. J. Brown, *J. Soc. Inform. Display*, 2006, **14**, 449.
4 (*a*) R. J. Holmes, B. W. D'Andrade, S. R. Forrest, X. Ren, J. Li and M. E. Thompson, *Appl. Phys. Letter.*, 2003, **83**, 3818; (*b*) S.-J. Yeh, M.-F. Wu, C.-T. Chen, Y.-H. Song, Y. Chi, M.-H. Ho, S.-F. Hsu and C. H. Chen, *Adv. Mater.*, 2005, **17**, 285; (*c*) C. S. K. Mak, A. Hayer, S. I. Pascu, S. E. Watkins, A. B. Holmes, A. Kohler and R. Friend, *Chem. Commun.*, 2002, 4708; (*d*) X. Zhang, C. Jiang, Y. Mo, Y. Xu, H. Shi and Y. Cao, *Appl. Phys. Letter.*, 2006, **88**, 051116; (*e*) L.-L. Wu, C.-H. Yang, I.-W. Sun, S.-Y. Chu, P.-C. Kao and H.-H. Huang, *Organometallic*, 2007, **26**, 2017; (*f*) P.-I. Shih, C.-H. Chien, C.-Y. Chuang, C.-F. Shu, C.-H. Yang, J.-H. Chen and Y. Chi, *J. Mater. Chem.*, 2007, **17**, 1692; (*g*) L. Chen, H. You, C. Yang, D. Ma and J. Qin, *Chem. Commun.*, 2007, 1352; (*h*) E. Orselli, G. S. Kottas, A. E. Konradsson, P. Coppo, R. Fröhlich, L. De Cola, A. van Dijken, M. Büchel and H. Börner, *Inorg. Chem.*, 2007, **46**, 11082.
5 (*a*) S.-J. Yeh, C.-T. Chen, Y.-H. Song, Y. Chi and M.-H. Ho, *J. Inform Display*, 2005, **13**, 857; (*b*) R. J. Holmes, S. R. Forrest, T. Sajoto, A. Tamayo, P. I. Djurovich, M. E. Thompson, J. Books, Y.-J. Tung, B. W. D'Andrade, M. S. Weaver, R. C. Kwong and J. J. Brown, *Appl. Phys. Lett.*, 2005, **87**, 243507; (*c*) C.-H. Yang, Y.-M. Cheng, Y. Chi, C.-J. Hsu, F.-C. Fang, K.-T. Wong, P.-T. Chou, C.-H. Chang, M.-H. Tsai and C.-C. Wu, *Angew. Chem. Int. Ed.*, 2007, **46**, 2418; (*d*) C.-F. Chang, Y.-M. C heng, Y. Chi, Y.-C. Chiu, C.-C. Lin, G.-H. Lee, P.-T. Chou, C.-C. Chen, C.-H. Chang and C.-C. Wu, *Angew. Chem. Int. Ed.*, 2008, **47**, 4542.
6 H. Y. Chen, W. Y. Lam, J. D. Luo, Y. L. Ho, B. Z. Tang, D. B. Zhu, M. Wong and H. S. Kwok, *Appl. Phys. Letter.*, 2002, **81**, 574.
7 (*a*) C.-C. Wu, Y.-T. Lin, K.-T. Wong, R.-T. Chen and Y.-Y. Chien, *Adv. Mater.*, 2004, **16**, 61; (*b*) M.-T. Lee, C.-H. Liao, C.-H. Tsai

and C. H. Chen, *Adv. Mater.*, 2005, **17**, 2493; (*c*) M.-F. Li, L. Wang, W.-K. Wong, K.-W. Cheah, H.-L. Tam, M.-T. Lee and C. H. Chen, *Appl. Phys. Lett.*, 2006, **89**, 121913; (*d*) H.-C. Li, Y.-P. Lin, P.-T. Chou, Y.-M. Cheng and R.-S. Liu, *Adv. Funct. Mater.*, 2007, **17**, 520; (*e*) C. J. Tonzola, A. P. Kulkarni, A. P. Gifford, W. Kaminsky and S. A. Jenekhe, *Adv. Funct. Mater.*, 2007, **17**, 863; (*f*) Y. Wai and C.-T. Chen, *J. Am. Chem. Soc.*, 2007, **129**, 7478; (*g*) P.-I. Shih, C.-Y. Chuang, C.-H. Chien, E. W.-G. Diau and C.-F. Shu, *Adv. Funct. Mater.*, 2007, **17**, 3141; (*h*) K.-C. Wu, P.-J. Ku, C.-S. Lin, H.-T. Shih, F.-I. Wu, M.-J. Huang, J.-J. Lin, I.-C. Chen and C.-H. Cheng, *Adv. Funct. Mater.*, 2008, **18**, 67; (*i*) S.-K. Kim, B. Yang, Y. Ma, J.-H. Lee and J.-W. Park, *J. Mater. Chem*, 2008, **18**, 3376; (*j*) Y.-Y. Lyu, J. Kwak, O. Kwon, S.-H. Lee, D. Kim, C. Lee and K. Char, *Adv. Mater.*, 2008, **20**, 2720; (*k*) S.-L. Lin, L.-H. Chan, R.-H. Lee, M.-Y. Yen, W.-J. Kuo, C.-T. Chen and R.-J. Jeng, *Adv. Mater.*, 2008, **20**, 3947.

8 (*a*) S.-C. Chang, G. He, F.-C. Chen, T.-F. Guo and Y. Yang, *Appl. Phys. Lett.*, 2001, **79**, 2088; (*b*) C.-C. Wu, T.-L. Liu, W.-Y. Hung, Y.-T. Lin, K.-T. Wong, R.-T. Chen, Y.-M. Chen and Y. Y. Chien, *J. Am. Chem. Soc.*, 2003, **125**, 3710.

9 S. C. Tse, K. C. Kwok and S. K. So, *Appl. Phys. Lett.*, 2006, **89**, 262102.

10 C.-L. Chiang, S.-M. Tseng, C.-T. Chen, C.-P. Hsu and C.-F. Shu, *Adv. Func. Mater.*, 2008, **18**, 248.

11 (*a*) K.-T. Wong, R.-T. Chen, F.-C. Fang, C.-C. Wu and Y.-T. Lin, *Org. Lett.*, 2005, **7**, 1979; (*b*) K.-T. Wong, R.-T. Chen, F.-C. Fang, C.-C. Wu and Y.-T. Lin, *Org. Lett.*, 2005, **7**, 5925; (*c*) K.-T. Wong, H.-F. Chen and F.-C. Fang, *Org. Lett.*, 2006, **8**, 3501.

12 (*a*) F. D. Libman and R. Slack, *J. Chem. Soc.*, 1951, 2588; (*b*) F. Dierschke, A. C. Grimsdale and K. Müllen, *Synthesis*, 2003, 2470.

13 C.-L. Chiang, C.-F. Shu and C.-T. Chen, *Org. Lett.*, 2005, **7**, 3717.

14 Crystal data for **PhSP$_{N2}$DPV·CH$_2$Cl$_2$**: $C_{50}H_{35}Cl_2N_3$: *Fw* = 748.71, monoclinoc, $P2_1/c$, Z = 4, $F(000)$ = 1560. Cell dimendions: a = 12.5133(3) Å, b = 34.5307(8) Å, c = 8.9169(2) Å, α = 90°, β = 100.493(2)°, γ = 90°, V = 3788.50(15) Å^3, $2\theta_{max}$ = 50.0°, ρ_{cacld} = 1.313 mg m^{-3}. Of 27836 reflections, 6695 were independence, 497 parameters, R (F_o) = 0.0392 (for reflections with $I > 2\sigma(I)$), R_w (F_o) = 0.0801 (for reflections with $I > 2\sigma(I)$). The GoF on F^2 was equal 0.776. Crystal data for **PhF$_{py2}$DPV**: $C_{49}H_{35}N_3$: *Fw* = 665.80, monoclinoc, $P2_1/c$, Z = 4, $F(000)$ = 1400. Cell dimendions: a = 13.1622(6) Å;, b = 25.6042(11) Å;, c = 10.9596(5) Å;, α = 90°, β = 107.046(2)°, γ = 90°, V = 3531.2(3) Å^3, $2\theta_{max}$ = 50.1°, ρ_{cacld} = 1.252 mg m^{-3}. Of 27399 reflections, 6169 were independence, 470 parameters, R (F_o) = 0.0395 (for reflections with $I > 2\sigma(I)$), R_w (F_o) = 0.0735 (for reflections with $I > 2\sigma(I)$). The GoF on F^2 was equal 0.685. CCDC-682902 and CCDC-682903 contain the supplementary crystallographic data of **PhSP$_{N2}$DPV·CH$_2$Cl$_2$** and PhF$_{py2}$DPV, respectively. These data can be obtained free of charge *via* www.ccd.cam.ac.uk/conts/retrieving.html (or from the Cambridge Crystallographic Data Centre, 12, Union Road, Cambridge CB21EZ, UK; fax: (+44)1223-336-033; or deposit@ccdc.cam.ac.uk).

15 A. D. Becke, *J. Chem. Phys.*, 1993, **98**, 5648.

16 M. E. Casida, In *Recent Advances in Density Functional Methods, Part 1*; D. P. Chong, Ed.; World Scientific: Singapore, 1995; p 155.

17 J. Kong, C. A. White, A. I. Krylov, C. D. Sherrill, R. D. Adamson, T. R. Furlani, M. S. Lee, A. M. Lee, S. R. Gwaltney, T. R. Adams, C. Ochsenfeld, A. T. B. Gilbert, G. S. Kedziora, V. A. Rassolov, D. R. Maurice, N. Nair, Y. Shao, N. A. Besley, P. E. Maslen, J. P. Dombroski, H. Daschel, W. Zhang, P. P. Korambath, J. Baker, E. F. C. Byrd, T. Van Voorhis, M. Oumi, S. Hirata, C.-P. Hsu, N. Ishikawa, J. Florian, A. Warshel, B. G. Johnson, P. M. W. Gill, M. Head-Gordon and J. A. Pople, *J. Comput. Chem.*, 2000, **21**, 1532.

18 K. Araki, L. Angnes and H. E. Toma, *Adv. Mater.*, 1995, **7**, 554.

19 M.-F. Wu, S.-J. Yeh, C.-T. Chen, H. Murayama, T. Tsuboi, W.-S. Li, I. Chao, S.-W. Liu and J.-K. Wang, *Adv. Funct. Mater.*, 2007, **17**, 1887.

20 M.-Y. Kuo, H.-Y. Chen and I. Chao, *Chem. Eur. J.*, 2007, **13**, 4750.

21 S. C. Tse, K. C. Kwok and S. K. So, *Appl. Phys. Lett.*, 2006, **89**, 262102.

22 (*a*) Z.-Y. Xie, T.-C. Wong, L.-S. Hung and S.-T. Lee, *Appl. Phys. Letter.*, 2002, **80**, 1477; (*b*) Y. Li, M. K. Fung, Z. Xie, S.-T. Lee, L.-S. Hung and J. Shi, *Adv. Mater.*, 2002, **14**, 1317.

23 (*a*) J. C. de Mello, H. F. Wittmann and R. H. Friend, *Adv. Mater.*, 1997, **9**, 230; (*b*) C.-L. Chiang, M.-F. Wu, D.-C. Dai, Y.-S. Wen, J.-K. Wang and C.-T. Chen, *Adv. Funct. Mater.*, 2005, **15**, 231.

24 (*a*) T. Yamamoto, M. Nishiyama and Y. Koie, *Tetragedron Lett.*, 1998, **39**, 2367; (*b*) J. Shi, C. W. Tang and C. H. Chen, U.S. Patent No. 5645948, 1997.

25 (*a*) D. L. White and J. W. Faller, *Inorg. Chem.*, 1982, **21**, 3119; (*b*) A. J. Canty, N. J. Minchin, L. M. Engelhardt, B. W. Skelton and A. H. White, *Aust. J. Chem.*, 1988, **41**, 651.

26 G. M. Sheldrick, *SHELXL-97*, University of Göttingen, Germany, 1997.

27 L. J. Farrugia, *J. Appl. Cryst.*, 1999, **32**, 837.

28 L.-H. Chan, R.-H. Lee, C.-F. Hsieh, H.-C. Yeh and C.-T. Chen, *J. Am. Chem. Soc.*, 2002, **124**, 6469.

29 S. R. Forrest, D. D. C. Bradley and M. E. Thompson, *Adv. Mater.*, 2003, **15**, 1043.

30 G. Wyszecki, W. S. Stiles, In *Color Science: Concepts and Methods, Quantitative Data and Formulae*; John Wiley & Sons: New York, 1982; p 259.